Journal Homepage: http://ijcpe.uobaghdad.edu.iq
Iraqi Journal of Chemical and Petroleum Engineering
Vol. 25 No. 3 (September 2024) 51 – 59
EISSN: 2618-0707, PISSN: 1997-4884

Study of adsorption isotherms and kinetics models for lead ions removal from simulated wastewater using three-dimensional, printed water-filtration system with synthesized α-Fe_2O_3

Noor M. Hammood [a, *], Nada N. Abdulrazzaq [a], Inen Akrouti [b]

a Department of Chemical Engineering, College of Engineering, University of Baghdad, Baghdad, Iraq
b Département de l'Education et l'enseignement, Institut Supérieur des Sciences Humaines de Jendouba ISSHJ, Université de Jendouba, Tunisia

Abstract

In this study, lead ions were removed from simulated wastewater by batch adsorptive filtration. A three-dimensional printed water filtration was designed using a blender and successfully synthesized from a PLA spool and a 3d printer machine. The filter surface was treated with NaOH solution to hydrolyze the polyester group in PLA. After that, α-Fe_2O_3 was prepared by the coprecipitation method and coated on the filter through doping and drying. α-Fe_2O_3 was characterized by X-ray diffraction (XRD), Energy-dispersive X-ray spectroscopy (EDX), and Brunauer-Emmet-teller (BET). The results successfully indicate the synthesis of α-Fe_2O_3 consisting of 67.3% Fe and 32.7% O_2. α-Fe_2O_3 appeared to have a surface area of 95 m^2/g with distinct morphology and functional group. The effect of initial Pb concentration (100-800) ppm and the effect of contact time (5-120) min on the removal process were studied. Lab data was collected, and the adsorption was investigated kinetically. The 3d printed filter system coated by iron oxide showed significant and promised results for wastewater treatment and lead ions removal using this technique. Also, the results showed that the adsorption of Pb ions on the α-Fe_2O_3 surface fitted with the Langmuir model, with a correlation coefficient (R^2) of 98.65%. The kinetic model's investigations revealed that the pseudo-second-order model was the most fitted model for the process with R^2 of 99.997%. The highest adsorption saturation capacity was 165.2 mg/g adsorbent.

Keywords: Chemical adsorption; α-Fe_2O_3 (Hematite); Co-precipitation; Polylactic acid (PLA); Adsorption Isotherms; Lead ions (II) removal; Wastewater treatment.

Received on 01/01/2024, Received in Revised Form on 14/05/2024, Accepted on 18/05/2024, Published on 30/09/2024

https://doi.org/10.31699/IJCPE.2024.3.6

1- Introduction

As the population grows, industries are developed to meet the needs of the people. This increase releases large amounts of wastewater that contain toxic, non-biodegradable heavy metals into the water, harming aquatic life, human health, and the environment. It is therefore imperative to treat the wastewater to remove it or bring its concentration down to an acceptable level using a variety of techniques [1]. The environment and human health are seriously threatened by heavy metal ions, which are poisonous, persistent, and build up in living things. Examples of these metals include arsenic, cadmium, chromium, lead, and mercury. These metals are especially dangerous because they cannot be recycled. Concern should be expressed about high concentrations of heavy metal ions in water systems, as they can result in a variety of health problems [2].

Pb (II) is the reason for Anemia, irreversible brain damage, kidney dysfunction, and various nervous system symptoms. Consequently, before releasing industrial wastewater into ecosystems, it must be treated to remove these hazardous metals [3]. The sustainable development goals of the UN state that the prevention of diseases will improve living circumstances through the preservation of natural resources [4]. The World Health Organization (WHO), the US Food and Drug Administration (FDA), and the European Protection Agency (EPA) are among the worldwide regulatory authorities that have established acceptable limits for lead ions in drinking water, which are 5 parts per billion (ppb) for bottled water, 10 parts per billion, and 15 parts per billion, respectively [5].

Numerous techniques, such as chemical precipitation, coagulation/flocculation, electrodialysis, electrochemical processes, ion exchange, adsorption, and membrane processes, have been employed to remove the toxicity of heavy metals from water [6]. Numerous factors, including waste type, contaminant concentration, required cleanup level, and economics, influence the choice of treatment [7]. Adsorption appears to hold the most promise due to its low cost, high efficiency, adaptable design, and simplicity of use. Because of their special qualities, such as a high specific surface area, many binding sites for the adsorbates to be adsorbed, multiple functional groups, and appropriate pore size, nanomaterials are favorable adsorbents in most typical adsorption systems. This

*Corresponding Author: Email: noor.moysar2107m@coeng.uobaghdad.edu.iq

makes them appealing adsorbents for the treatment of heavy metal-polluted industrial wastewater [8].

It is commonly known that the adsorption process is greatly influenced by the type of adsorbent used [9]. Researchers have used a wide range of adsorbent materials to remove Pb(II) and other metals from an aqueous medium. These materials include rice husk modified by phosphoric acid (PRH), Schiff's base ZnO/aminated chitosan, DSDH ligand, thiosemicarbazone modified chitosan, green reduced graphene oxide, UiO-66-NH_2 MOF, activated carbon, and arginine modified activated carbon [10]. Metal oxides have a high affinity for metal ions and are inexpensive to produce, making them an excellent Pb-adsorbent candidate. In comparison to bulk materials, nanostructured metal oxide adsorbents are more suitable for heavy metal ion removal because they typically have a high surface area, controllable pore size distribution, mass transfer promotion, and a large number of surface-active sites [11].

Iron oxide-based materials are promising for the removal of various organic and inorganic pollutants, because of their stable structure and abundance on Earth. Ferric oxide (Fe_2O_3) has multiple crystal structures under natural conditions, including α -Fe_2O_3, β -Fe_2O_3, γ -Fe_2O_3, and σ -Fe_2O_3 [12]. Iron oxide-modified media was highly investigated, such as cement, iron-oxide-coated zeolite, activated carbon, activated alumina, biomasses, polymers, and carbon nanotubes (CNTs) [13].

3D printing is a potentially useful technology for meeting the need for a low-cost, electricity-free process for filtering arsenic from water. 3D printing allows for the rapid production of small quantities of robust, innovative, and customized goods at low cost, as well as the production of customized and complex objects on micrometer-to-millimeter scales. Also, the technology can be used without the need for traditional industrial processes such as molding or milling [14]. "3D printed reaction ware" is a term used to describe a 3D printed device used in chemical reactions. Such three-dimensional printed reaction ware holds promise as an inexpensive, automated, and reversible chemical reaction platform. Plastic is one material that can be employed as reaction ware in 3D printing because it is inexpensive and widely available.

Fused Deposition Modeling (FDM) is a widely used printing technique that entails melting thermoplastics using a heated nozzle and depositing the melted material in layers. Therefore, shortages in the supply of necessities in developing nations can be filled by producing desired products on demand at a low cost through customization [13]. PLA is the most widely used material for FDM due to its ease of processing and commercial availability which became popular in wastewater treatment recently [15], (Kihoon Kim) manufactured a 3D printed filter system from PLA using a 3D printer for the removal of arsenic from wastewater [16]. Another researcher used PLA to manufacture a 3D-printed biodegradable membrane and compared it to conventional PLA membranes [17]. PLA is known as a biodegradable primary biopolymer derived from renewable resources, including sugarcane or maize starch. It is a thermoplastic that degrades naturally and has strong absorbability and biocompatibility qualities. With a glass transition temperature (T_g) of 55 to 59 °C and a melting temperature (Tm) of 170 to 180 °C, PLA is regarded as a semicrystalline polymer [18]. Bioplastics or biodegradable polymers are promising candidates to replace fossil-based plastics since they use renewable resources and have much lower greenhouse gas emissions (GHE) [19].

In this research, a 3D-printed water filtration system was manufactured, hydrolyzed, and coated by synthesized α-Fe_2O_3 following the method mentioned in the literature [13]. After that, a study was done on the effect of initial concentration and contact time on the removal of Pb ions from wastewater by batch adsorptive filtration. Finally, several adsorption isotherms and kinetic models were investigated to describe the process.

2- Experimental work

2.1. Materials

All materials that were purchased and used during the experiments are listed in Table 1.

Table 1. The Materials that were used for the Study Work

Material	Chemical Formula	Appearance	Supplier
Hydrochloric acid	HCl 32%	Liquid	BHD laboratory
Sodium hydroxide	NaOH	White powder	Sigma-Aldrich
Distilled water	H_2O	Liquid	University Lab
Lead nitrate	Pb $(NO_3)_2$	White powder	Sigma-Aldrich
PLA spool	N/A	White solid	Creality
Iron chloride (III)	$FeCl_3$	Black powder	Eisen-Golden Laboratories

2.2. Laboratory apparatus and equipment

The laboratory apparatus and equipment used in this research are listed in Table 2 as follows:

Table 2. Laboratory Apparatus and Equipment

No.	Laboratory Apparatus or Equipment	Model or Origin	Function
1	Oven	Italy	Heating
2	3D printing machine	Ender 3 v2 neo/ China	Manufacturing of filters
3	Magnetic stirrer	China	Homogenizing solution with or without heating
4	PH meter	USA	pH level measuring

2.3. 3D printed filter manufacturing.

The model of the filter was designed using the blender app. The filter dimensions were 50 mm in diameter and 50 mm in height. The designed models have been exported from Blender in (STL) form data to be imported

to a reality 3D printer machine. The 3D printer that was used has a nozzle of (0.4 mm) for melting and depositing the PLA filament through the calculated pathway and fabrication filter with 70% infill as shown in Fig. 1 3D printed filters.

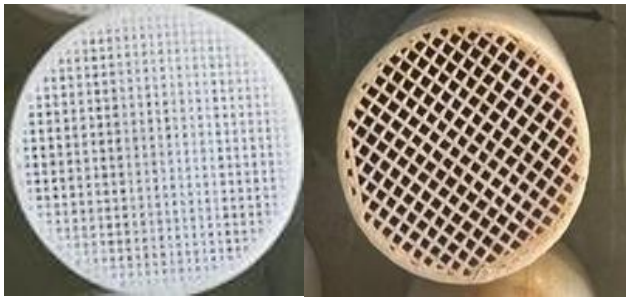

Fig. 1. 3D Printed and Coated Filter by Iron oxide

2.4. Adsorbent preparation

Adsorbent preparation was done following the work of (Kihoon Kim). The iron hydroxide was synthesized by a simple co-precipitation method under mild conditions. In an aqueous solution, $FeCl_3$ and NaOH were combined to precipitate $Fe(OH)_3$. 400 ml of $FeCl_3$ (0.025 M) was mixed for a minute at 700 rpm, while 300 ml NaOH (0.025 M) was added to the solution during stirring. Since $Fe(OH)_3$ particles are highly insoluble in water, insolubility is maximized by adjusting the pH to raise the amount of $Fe(OH)_3$ that was deposited onto the filters. By gently adding 0.1 M of each NaOH and HCl to the solution and stirring, the pH was brought to 8.0. $Fe(OH)_3$ particles were precipitated to the beaker's bottom within minutes. After removing the supernatant, the concentration of $Fe(OH)_3$ was increased until 300 mL of solution was left.

2.5. Hydrolyzing and α-Fe_2O_3 coating of filters

Following the procedure of [13]. Iron oxide coating and hydrolysis were used for surface treatment. For hydrolyzing of the polyester group, which was presented in PLA, a solution of NaOH (10 M) has been poured throughout the filter's channels. After that, the 3D-printed PLA filters were repeatedly dipped into and removed from the solution. The filters underwent a 12-hour drying process at 60 ºC in an oven to convert iron (III) hydroxide to iron oxide (hematite). 1 L of tap water was run across each filter following the drying process to remove the excess amount of α-Fe_2O_3 nanoparticles from the filter. Again, the steps of soaking, lifting, drying, and washing were carried out. The adsorption of iron (III) oxide appears as rust on the filter's surface, which is brown due to the iron (III) oxide solution's initial brown color. This color shift indicates the adsorption of iron (III) oxide onto the filter. The filter was weighed up both before and after the loading procedure to allow us to calculate the amount of α-Fe_2O_3 that was loaded onto it all process as displayed in Fig. 2. The coating process was repeated several times to increase the amount of α-Fe_2O_3

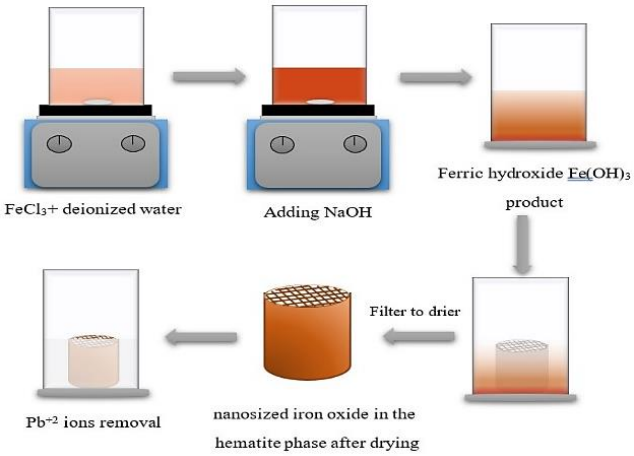

Fig. 2. Schematic Diagram of the Experimental Setup

2.6. Batch Adsorption of Pb ions

Different amounts of $Pb(NO_3)_2$ were mixed with distilled water to prepare simulated wastewater lead samples with concentrations of 100-800 ppm. The batch adsorption experiments were performed in a 500 ml glass bottle placed in a shaker. A 3D-printed filter containing 1 g of α-Fe_2O_3 was immersed in 250 ml of simulated wastewater, and the pH level was adjusted to 6.5. After preparing the samples in the flaxes, they were closed to prevent spilling throughout the shaking. The mixture was shaken at a constant rotation speed of 150 rpm. Adsorption treatment started by varying the initial concentration of Pb ions within the range of 100-800 ppm for 120 min then the effect of contact time was studied within the range of 5-120 min. After that, the samples were analyzed by atomic adsorption spectrophotometer (AAS) to determine the concentration of residual Pb ions. Finally, the percentage of removal (%R) and adsorption capacities (q_e and q_t) of Pb ions were calculated using the following equations:

$$\%R = \frac{C_o - C}{C_o} * 100 \quad (1)$$

$$qe = \frac{Co - Ce}{m} x\, V \quad at\ constant\ mixing\ time \quad (2)$$

$$qt = \frac{Co - Ct}{m} x\, V \quad at\ different\ \ mixing\ time \quad (3)$$

Where: C_o: the initial Pb ions content in simulated wastewater. C: the measured Pb ions content in simulated wastewater. q_e: adsorption capacity at equilibrium mg/g. q_t: adsorption capacity at sampling time mg/g. V: volume of wastewater in Liter. M: mass of adsorbent in grams. C_o, C_e, and C_t are Pb ions content at initial, equilibrium, and intervals sampling time respectively in ppm.

2.7. Adsorption isotherm models

Adsorption isotherms provide a clear description of the relationship between the quantity of the adsorbent (q_e) and the remaining content of the adsorbate (C_e) under equilibrium state and constant temperature conditions [20]. By utilizing adsorption isotherms, one can fully

understand the relationship between the dissolved compounds and the adsorbent in the solution, determine the ideal adsorption conditions by examining the nature of adsorption, and quantify the adsorbate concentration in the case of a liquid and the pressure in the case of gas [21]. Additionally, when the process reaches an equilibrium state, adsorption isotherms illustrate how molecules are distributed in the medium of the liquid and solid phases. The phenomenon of adsorption is classified based on the relationship between the quantity of adsorbate and the surface temperature of the adsorbent. However, as new equilibrium forms, the concentration also changes proportionately [21].

The Langmuir model allows for the determination of whether a monolayer is adsorbed or not; otherwise, no contact between the adsorbed molecules is possible. The Langmuir equation holds for a single monolayer adsorbed with a well-defined number of energetically identical and uniform adsorption sites [22]. Eq. 4 and Eq. 5 are the mathematical equations that describe the Langmuir adsorption isotherm for the linear case [8].

$$q_e = \frac{q_{max} . K_L C_e}{1 + K_L C_e} \quad (4)$$

$$\frac{1}{q_e} = \frac{1}{q_{max} K_L} \frac{1}{C_e} + \frac{1}{q_{max}} \quad (5)$$

Where: q_e: adsorption capacity when equilibrium is achieved described by units of mg/g. C_e: the adsorbed concentration at equilibrium by units of mg/l. q_{max}: adsorption capacity at maximum by units of mg/g. K_L: the Langmuir constant expressed the binding sites in units of l/mg.

The Freundlich model assumed that the adsorption process occurs in a multilayer suspension and that the molecular distribution is heterogeneous on the adsorbent's surface [9]. Eq. 6 is a mathematical illustration of the isotherm. Whereas Eq. 7 is the linear form of the Freundlich isotherm model [23].

$$q_e = K_F \, C_e^{\frac{1}{n}} \quad (6)$$

$$\ln q_e = \ln K_F + \frac{1}{n} \ln C_e \quad (7)$$

Where: q_e: represents adsorption capacity when equilibrium is reached (mg/g). K_F: is known as the Freundlich constant which represents the calculated capacity of adsorption [$(mg.g^{-1}).(mg^{-1})^{1/n}$]. n: is the intensity value for adsorption which determines adsorption type.

Temkin's model describes adsorption as a uniform distribution of binding energy up to the maximum value. The quantity of metal ions adsorbed was directly correlated with the number of active sites on the surface of the adsorbent material. Using Temkin's model, we can determine the adsorption energy and the interactions between ions and GO. [8]. To apply the Temkin isotherm, use Eq. 8 [24].

$$q_e = B \ln K_T + B \ln C_e \quad (8)$$

Where B and K_T are the Temkin energy constant (J/mol) and the constant describing the interaction between Pb molecules and adsorbent surface (dimensionless), respectively.

2.8. Adsorption kinetic models

The rate at which contaminants move from the liquid phase to the adsorbent surface at variable values is known as the adsorption kinetic. The goal of studying adsorption kinetics is to predict the mechanism underlying adsorption phenomena. Primarily, the pseudo-first-order model and pseudo-second-order model are utilized to examine adsorption kinetics [8, 25].

The pseudo-first-order assumed that adsorption was thought to form in a single layer on the surface of adsorption between the liquid and solid phases, additionally, to depict the initial stages of adsorption phenomena, the pseudo-first-order model was assumed. This model is represented by Eq. 9 [8]

$$ln\,(q_e - q_t) = ln\, q_e - k_1 t \quad (9)$$

Where: q_t is the adsorbate quantity that the adsorbent takes in a specific time (mg/g), q_e is adsorption capacity at equilibrium (mg/g) and k_1 is the rate constant (1/min).

The pseudo-second-order kinetic model forecasts behavior across the entire adsorption range based on the supposition that chemical sorption, or chemisorption, is the rate-limiting step, under these circumstances, the adsorption rate depends more on the adsorption capacity than the adsorbate concentration. The linearized Eq. 10 of this model is stated as follows [26].

$$\frac{t}{q_t} = \frac{1}{k_2 q_e^{\,2}} + \frac{1}{q_e} t \quad (10)$$

Where: q_t: the amount of adsorbate which adsorbent adsorbed in a specific time (mg/g). q_e: Capacity of adsorption at equilibrium (mg/g). K_2: Constant rate (1/min).

3- Results and discussion

3.1. Characterization of adsorbent

The crystallographic characteristics of α-Fe_2O_3 were examined by XRD; the synthesized powder sample's XRD pattern is displayed in Fig. 3. The peaks that show up at 24.16°, 33.12°, 35.63°, 40.64°, 49.47°, 54.08°, and 57.42° are the pure α-Fe_2O_3 nanoparticles' 012, 104, 110, 113, 024, 116, 214, 300, 028, 119, and 200 crystalline structures. The formation of the hematite phase is indicated by the highest peak in the XRD pattern of pure α–Fe_2O_3, which is located at approximately 33° and corresponds to the (104) plane. There was no peak visible that corresponded to the other phases of the iron oxide. The hematite products' narrow and sharp peaks suggested that they were highly crystalline, which suggested that this preparation method is responsible for the high purity of the synthesized hematite particles. The result agrees

with these previous studies [27, 28]. BET technique revealed that the surface area of the synthesized α-Fe_2O_3 was 95 m^2/g. The synthesized α-Fe_2O_3 appeared to consist of 67.3% Fe and 32.7% O_2 as indicated by the EDX technique.

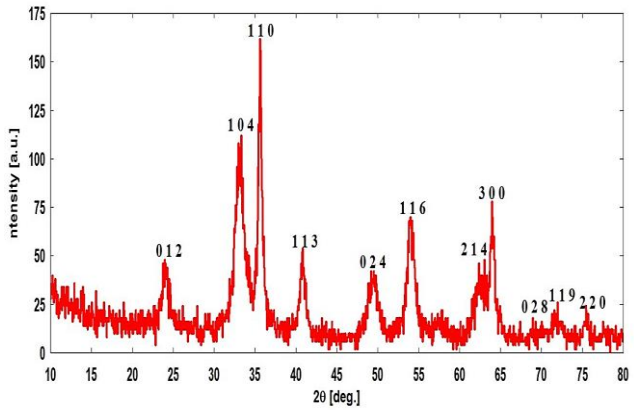

Fig. 3. XRD Pattern of Synthesized α-Fe2O

3.2. Effect of initial concentration

Fig. 4 illustrates the effect of the initial concentration of Pb ions on the adsorption within the range of (100-800) ppm under the conditions of 120 min of contact time, room temperature, 150 rpm speed of shaking, 1 g of α-Fe_2O_3 adsorbent coated on the filter's surface area, and the volume of simulated wastewater was 250 ml. The removal efficiency of Pb ions was more than 99% for the initial concentrations within a range of 100-200 ppm while it decreased to 82.6% at 800 ppm. The highest removal achieved was 99.4 at 100 ppm while the highest capacity was 165.2 mg/g at 800 ppm, this result was close to an earlier study [29]. Where adsorption capacity was found to be 169.49 mg/g. This can be attributed to the high quantity of adsorbent active sites compared to the amount of Pb ions presented in the solution.

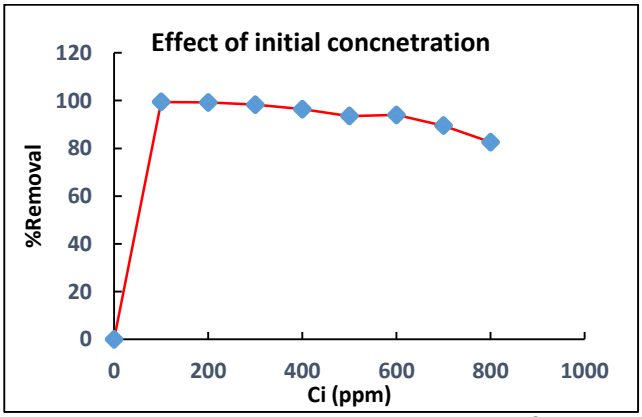

Fig. 4. The Effect of Initial Concentration of Pb^{+2} Ions on the Removal Efficiency

3.3. Effect of contact time

Fig. 5 shows the effect of contact time within a range of 5-120 min on the efficiency of removal of Pb ions under conditions of 800 ppm of Pb, 150 rpm of shaking speed, 1 g of α-Fe_2O_3 adsorbent coated on the filter's surface area, and the volume of simulated wastewater was 250 ml. Most of the removal occurred within the first 5 minutes of the process. A fast adsorption of Pb with 77.8% removal from 800 ppm to 177.6 ppm was achieved after 5 minutes while it reached about 82.6% after 120 min. It is obvious that the highest removal efficiency occurred in the first five minutes then the process efficiency decreased. At the beginning of the process, there was the access of α-Fe_2O_3 active sites to adsorb Pb ions but as time passed, the equilibrium was reached and the active sites became saturated and had no more ability to adsorb the ions [30, 31]

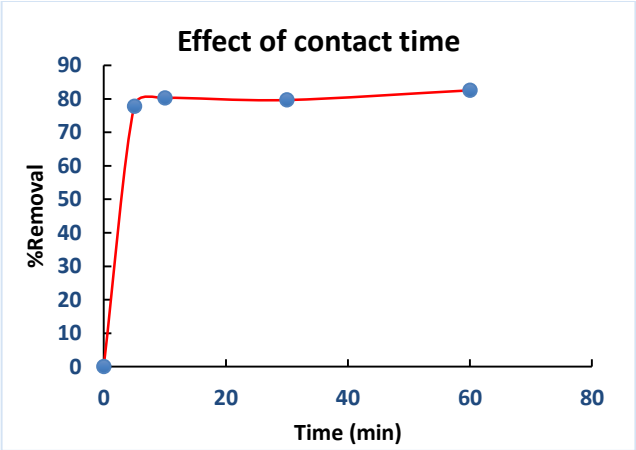

Fig. 5. Effect of Contact Time on the Removal Efficiency

3.4. Isotherm model

The application of Eqs. 5, 7, and 8 results in Fig. 6, Fig. 7, and Fig. 8 display the parameters and correlation coefficients for each adsorption isotherm. Table 3 shows that the Langmuir isotherm was the most appropriate for Pb ions removal since R^2 (98.65%) was the closest to unity. This result is in line with the previous works [29, 32, 33]. For the specified concentration range, the Langmuir isotherm confirms the presence of the adsorbate monolayer (Pb) at the adsorbent surface. According to the Freundlich adsorption isotherm equation, n had a value of 2.97.

Table 3. Parameters of Adsorption Isotherms

Langmuir			Freundlich			Temkin		
KL	qm	R^2	KF	n	R^2	BT	KT	R^2
0.376885	133.333	98.65%	37.222	2.97	95.41%	34.744	0.999	97.77%

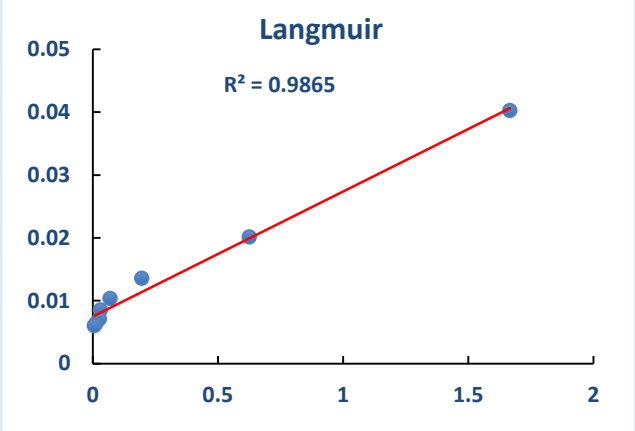

Fig. 6. Adsorption Isotherm Model Langmuir

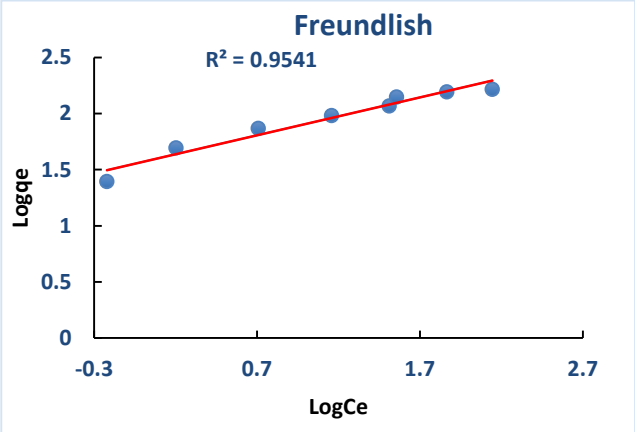

Fig. 7. Adsorption Isotherm Model Freundlich

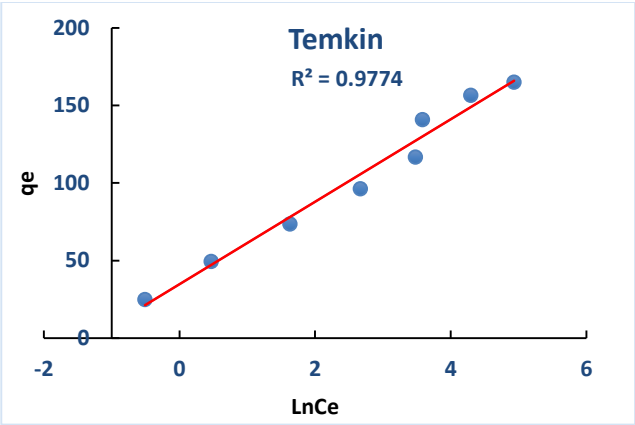

Fig. 8. Adsorption Isotherm Temkin

3.5. Kinetic model

Two commonly used models, the pseudo-first order and pseudo-second-order models, have been used to calculate the kinetic data for the adsorption of Pb ions on Fe_2O_3 as an adsorbent. The two applied models' correlation factors and other parameters are listed in Table 4. As can be seen from Fig. 9, and Fig. 10, the pseudo-second-order model, which has the highest correlation factor for applied models, was very close to unity (99.997%), making it the best model to represent and describe the experimental data. The pseudo-second-order was a good model to describe Pb ions removal by adsorption, according to several prior studies [11, 29].

Table 4. Parameters of Kinetic Models

Pseudo-1st order			Pseudo-2nd order		
qe	K1	R^2	qe	K2	R^2
13.1602	0.00028	20.05%	163.934	0.01861	99.997%

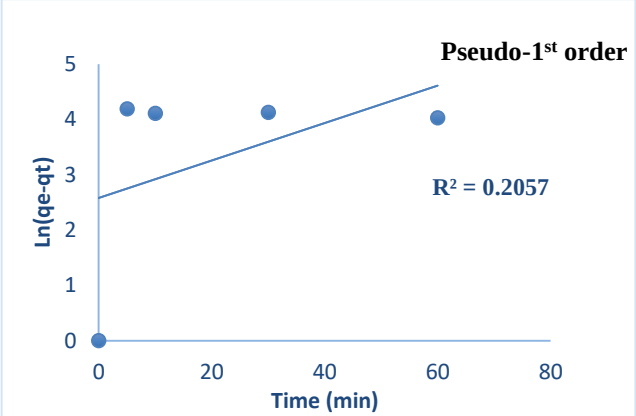

Fig. 9. The Pseudo-First-Order Model of Pb(II)Ion Adsorption

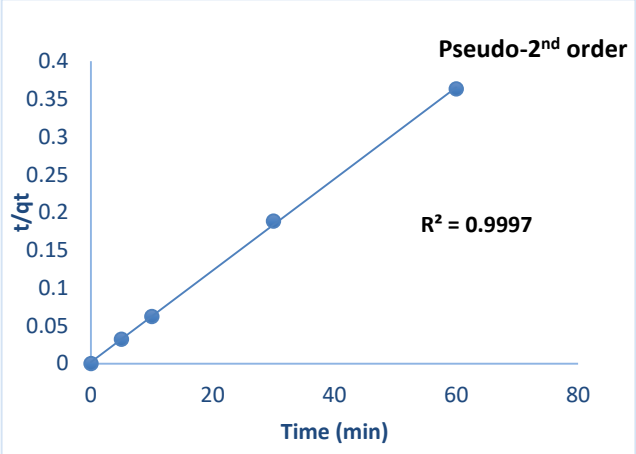

Fig. 10. The Pseudo-Second-order Model Pb(II)Ion Adsorption

4- Conclusion

Characterization techniques confirmed the successfully synthesized of α -Fe_2O_3. XRD phase pattern showed the exact peaks of α -Fe_2O_3, and the surface area was 300 m^2/g as a result of the BET. High and fast removal of Pb ions was achieved, the 3d filtration system coated with α -Fe_2O_3 could achieve 99% removal for 100-200 ppm of Pb ions while it decreased to 82.6% for an initial concentration of 800 ppm. The adsorbent had a Pb ions adsorption capacity of 165.2 mg/g which is higher than the previous studies. The Langmuir isotherm was the most fitted to describe the adsorption process with R^2 of 98.65%. Also, the studied kinetic models indicate that the adsorption removal followed the pseudo-second-order with R^2 of 99.997%.

Acknowledgment

We would like to express our deepest gratitude to the Chemical Engineering Department, College of Engineering, University of Baghdad, for their invaluable support and resources in making this research possible. Their expertise and guidance played a crucial role in our success.

References

[1] Z. M. Issa and R. H. Salman, "Chromium Ions Removal by Capacitive Deionization Process: Optimization of the Operating Parameters with Response Surface Methodology," *Journal of Ecological Engineering*, vol. 24, no. 1, pp. 51–65. 2023, https://doi.org/10.12911/22998993/155953

[2] H. N. A. Alhuseen and N. N. Abdulrazzaq, "Flotation of Cadmium Ions from Wastewater Using Air Micro-Bubbles," *Journal of Ecological Engineering*, vol. 24, no. 8, pp. 95–105, June 2023, https://doi.org/10.12911/22998993/166062

[3] H. N. Abdulameer and S. M. Al-Jubouri, "A Comparison Study for The Performance of Polyethersulfone Ultrafiltration Mixed Matrix Membranes in The Removal of Heavy Metal Ions from Aqueous Solutions," I*raqi Journal of Chemical and Petroleum Engineering*, vol. 23, no. 2, pp. 19–25, June 2022, https://doi.org/10.31699/IJCPE.2022.2.3

[4] J. R. Njimou, M. Pengou, H. K. Tchakoute, M. S. Tamwa, C. Tizaoui, U. Fannang, P. N. Lemougna, C. P. Nanseu-Njiki and E. Ngameni, "Removal of lead ions from aqueous solution using phosphate-based geopolymer cement composite," *Journal of Chemical Technology & Biotechnology*, vol. 96, no. 5, pp. 1358–1369, Jan. 2021, https://doi.org/10.1002/jctb.6657

[5] S. Singh, D. Bhatt, A. Deep, and U. K. Tiwari, "An antibody conjugated NH2-MIL-101(Fe) metal-organic framework based optical biosensor for sensitive detection of lead ions," *Microchemical Journal*, vol. 199, p. 110122, Apr. 2024, https://doi.org/10.1016/j.microc.2024.110122

[6] N. H. Ibrahim and S. M. Al-Jubouri, "Facile preparation of dual functions zeolite-carbon composite for zinc ion removal from aqueous solutions," *Asia-Pacific Journal of Chemical Engineering*, Aug. 2023, https://doi.org/10.1002/apj.2967

[7] A. I. Alwared, N. Abdulrazzaq, and B. Al-Sabbagh, "Micro-Bubble Flotation for Removing Cadmium Ions from Aqueous Solution: Artificial Neural Network Modeling and Kinetic of Flotation," *Iraqi Journal of Chemical and Petroleum Engineering*, vol. 20, no. 2, pp. 1–9, June 2019, https://doi.org/10.31699/IJCPE.2019.2.1

[8] N. Jawad and T. M. Naife, "Mathematical Modeling and Kinetics of Removing Metal Ions from Industrial Wastewater," *Iraqi Journal of Chemical and Petroleum Engineering*, vol. 23, no. 4, pp. 59–69, 2022, https://doi.org/10.31699/IJCPE.2022.4.8

[9] Z. N. Jamka and W. T. Mohammed, "Assessment of the Feasibility of Modified Chitosan Beads for the Adsorption of Nitrate from an Aqueous Solution," *Journal of Ecological Engineering*, vol. 24, no. 2, pp. 265–278, Jan. 2023, https://doi.org/10.12911/22998993/156886

[10] A. A. Alqadami, M. Naushad, Z. A. ALOthman, M. Alsuhybani, and M. Algamdi, "Excellent adsorptive performance of a new nanocomposite for removal of toxic Pb(II) from aqueous environment: Adsorption mechanism and modeling analysis," *Journal of Hazardous Materials*, vol. 389, p. 121896, Dec. 2020, https://doi.org/10.1016/j.jhazmat.2019.121896

[11] J. Chang, J. Wang, J Qu, Y. V. Li, L. Ma, L. Wang, X. Wanga and K. Pan, "Preparation of α-Fe2O3/polyacrylonitrile nanofiber mat as an effective lead adsorbent," *Environmental Science: Nano*, vol. 3, no. 4, pp. 894–901, June 2016, https://doi.org/10.1039/C6EN00088F

[12] W. Chen, Z. Lu, B. Xiao, P. Gu, W. Yao, J. Xing, A. M. Asiri, K. A. Alamry, X. Wang and S. Wang "Enhanced removal of lead ions from aqueous solution by iron oxide nanomaterials with cobalt and nickel doping," *Journal of Cleaner Production*, vol. 211, pp. 1250–1258, Feb. 2019, https://doi.org/10.1016/j.jclepro.2018.11.254

[13] K. Kim, M. C. Ratri, G. Choe, M. Nam, D. Cho, and K. Shin, "Three-dimensional, printed water-filtration system for economical, on-site arsenic removal," *PLoS ONE*, vol. 15, no. 4, pp. 1–15, Apr. 2020, https://doi.org/10.1371/journal.pone.0231475

[14] C. Weller, R. Kleer, and F. T. Piller, "Economic implications of 3D printing: Market structure models in light of additive manufacturing revisited," *International Journal of Production Economics*, vol. 164, pp. 43–56, June 2015, https://doi.org/10.1016/j.ijpe.2015.02.020

[15] H. He, M. Gao, B. Illés, and K. Molnar, "3D Printed and electrospun, transparent, hierarchical polylactic acid mask nanoporous filter," *International Journal of Bioprinting*, vol. 6, no. 4, pp. 1–9, Jul. 2020, https://doi.org/10.18063%2Fijb.v6i4.278

[16] K. Kim, M. C. Ratri, G. Choe, M. Nam, D. Cho, and K. Shin, "Three-dimensional, printed water-filtration system for economical, on-site arsenic removal," *PLoS ONE*, vol. 15, no. 4, pp. 1–15, Apr. 2020, https://doi.org/10.1371/journal.pone.0231475

[17] H. Y. Zhang, H. B. Jiang, J. H. Ryu, H. Kang, K. M. Kim, and J. S. Kwon, "Comparing properties of variable pore-sized 3D-printed PLA membrane with conventional PLA membrane for guided bone/tissue regeneration," *Materials*, vol. 12, no. 10, pp. 1–11, May 2019, https://doi.org/10.3390/ma12101718

[18] S. Bandehali, H. Sanaeepur, A. Ebadi Amooghin, S. Shirazian, and S. Ramakrishna, "Biodegradable polymers for membrane separation," *Separation and Purification Technology*, vol. 269, p. 118731, Aug.2021, https://doi.org/10.1016/j.seppur.2021.118731

[19] E. Rezvani Ghomi, F. Khosravi, A. S. Ardahaei,Y. Dai, R. E. Neisiany, F. Foroughi, M. Wu, O. Das, and S. Ramakrishna, "The life cycle assessment for polylactic acid (PLA) to make it a low-carbon material," *Polymers*, vol. 13, no. 11, pp. 1–16, June 2021, https://doi.org/10.3390/polym13111854

[20] B. D. Radhi and W. T. Mohammed, "Novel nanocomposite adsorbent for desulfurization of 4,6-dimethyldibenzothiophene from model fuel," *Materials Today: Proceedings*, vol. 42, pp. 2880–2886, Mar. 2021, https://doi.org/10.1016/j.matpr.2020.12.738

[21] N. Gaur, K. Narasimhulu, and Y. PydiSetty, "Recent advances in the bio-remediation of persistent organic pollutants and its effect on environment," *Journal of Cleaner Production*, vol. 198, pp. 1602–1631, July 2018, https://doi.org/10.1016/j.jclepro.2018.07.076

[22] G. K. Jabaar, H. A. Al-jendeel, and Y. Ali, "Desulphurization of Simulated Oil Using SAPO-11 with CNT' s as Adsorbent: A Kinetic Study," *Iraqi Journal of Chemical and Petroleum Engineering*, vol. 24, no. 3, pp. 69–77, Sept. 2023, https://doi.org/10.31699/IJCPE.2023.3.7

[23] S. M. Al-Jubouri, H. A. Al-Jendeel, S. A. Rashid, and S. Al-Batty, "Green synthesis of porous carbon cross-linked Y zeolite nanocrystals material and its performance for adsorptive removal of a methyl violet dye from water," *Microporous and Mesoporous Materials*, vol. 356, p. 112587, Apr. 2023, https://doi.org/10.1016/j.micromeso.2023.112587

[24] M. S. Abdulrahman, A. A. Alsarayreh, S. K. A. Barno, M. A. Abd Elkawi, and A. S. Abbas, "Activated carbon from sugarcane as an efficient adsorbent for phenol from petroleum refinery wastewater: Equilibrium, kinetic, and thermodynamic study," *Open Engineering*, vol. 13, no. 1, June 2023, https://doi.org/10.1515/eng-2022-0442

[25] M. Al-Jabari, "Kinetic models for adsorption on mineral particles comparison between Langmuir kinetics and mass transfer," *Environmental Technology and Innovation*, vol. 6, pp. 27–37, 2016, https://doi.org/10.1016/j.eti.2016.04.005

[26] T. R. Sahoo and B. Prelot, "Adsorption processes for the removal of contaminants from wastewater: The perspective role of nanomaterials and nanotechnology," in *Nanomaterials for the Detection and Removal of Wastewater Pollutants, 1st ed., Amsterdam, Netherlands: Elsevier Inc.*, Jun. 2020, https://doi.org/10.1016/B978-0-12-818489-9.00007-4

[27] A. Lassoued, B. Dkhil, A. Gadri, and S. Ammar, "Control of the shape and size of iron oxide (α-Fe2O3) nanoparticles synthesized through the chemical precipitation method," *Results in Physics*, vol. 7, pp. 3007–3015, Sept. 2017, https://doi.org/10.1016/j.rinp.2017.07.066

[28] V. Kumar, S. Chahal, D. Singh, A. Kumar, P. Kumar, and K. Asokan, "Annealing effect on the structural and dielectric properties of hematite nanoparticles," *AIP Conference Proceedings*, vol. 1953, 2018, https://doi.org/10.1063/1.5032580

[29] H. J. Kim, J. M. Lee, J. H. Choi, D. H. Kim, G. S. Han, and H. S. Jung, "Synthesis and adsorption properties of gelatin-conjugated hematite (α-Fe2O3) nanoparticles for lead removal from wastewater," *Journal of Hazardous Materials*, vol. 416, p. 125696, Apr. 2021, https://doi.org/10.1016/j.jhazmat.2021.125696

[30] Y. G. Chen, W. M. Ye, X. M. Yang, F. Y. Deng, and Y. He, "Effect of contact time, pH, and ionic strength on Cd(II) adsorption from aqueous solution onto bentonite from Gaomiaozi, China," *Environmental Earth Sciences*, vol. 64, no. 2, pp. 329–336, Nov. 2011, http://dx.doi.org/10.1007/s12665-010-0850-6

[31] D. M. G. Saad, E. M. Cukrowska, and H. Tutu, "Phosphonated cross-linked polyethylenimine for selective removal of uranium ions from aqueous solutions," *Water Science and Technology*, vol. 66, no. 1, pp. 122–129, July 2012, https://doi.org/10.2166/wst.2012.133

[32] B. Tsedenbal, J. E. Lee, M. S. Kim, S. H. Huh, and B. H. Koo, "Flower-Like α -Fe 2 O 3 for Removal of Heavy Metals from Wastewater," *Journal of Nanoscience and Nanotechnology*, vol. 20, no. 11, pp. 6753–6759, Nov. 2020, https://doi.org/10.1166/jnn.2020.18796

[33] M. Hashemzadeh, A. Nilchi, and A. H. Hassani, "Synthesis of novel surface-modified hematite nanoparticles for lead ions removal from aqueous solution," *Materials Chemistry and Physics*, vol. 227, pp. 279–290, Feb. 2019, https://doi.org/10.1016/j.matchemphys.2019.02.025

دراسة موديلات الايزوثيرم وموديلات الامتزاز الحركية لإزالة أيونات الرصاص من محاكاة مياه الصرف الصحي باستخدام نظام ترشيح المياه المطبوع ثلاثي الأبعاد مع $\alpha-Fe_2O_3$ المصنع

نور ميسر حمود [١،*]، **ندى نعوم عبد الرزاق** [١]، **عفان عكروتي** [٢]

١ قسم الهندسة الكيمياوية، كلية الهندسة، جامعة بغداد، بغداد، العراق
٢ قسم التربية والتعليم، المعهد العالي للعلوم الانسانية بجندوبة، جامعة جندوبة، تونس

الخلاصة

في هذه الدراسة تمت ازالة أيونات الرصاصص بمحاكاة مياه الصرف بواسطة الترشيح الامتزازي. تم تصميم نظام ثلاثي الابعاد لترشيح المياه باستخدام برنامج Blender ثم تمت عملية التصنيع من بكرة (PLA) وباستخدام طابعة ثلاثية الابعاد. تمت معالجة سطح الفلتر بمحلول NaOH لتحليل مجموعة البوليستر في PLA. بعد ذلك، تم تحضير ($\alpha-Fe2O3$) النانوية طريقة الترسيب المشترك وطلائه على المرشح من خلال غمر الفلتر في محلول هيدروكسيد الحديد الثلاثي $Fe(OH)_3$وتجفيف الفلتر ليتحول هيدروكسيد الحديد الثلاثي الى أوكسيد الحديد (الهيماتيت) النانو تم تشخيص $\alpha-Fe_2O_3$ بواسطة حيود الأشعة السينية (XRD)، و(BET) Brunauer–Emmet–teller و(EDX)Energy–dispersive X–ray spectroscopy. تشير النتائج الى نجاح تصنيع $\alpha-Fe_2O_3$ وبتركيب يتكون من ٣٢,٧% حديد و٦٧,٣% أوكسجين, وبمساحة سطحية تبلغ 95 م²/جم. تمت دراسة تأثير تركيز الرصاص الأولي (١٠٠–٨٠٠) جزء في المليون وزمن التلامس (٥–١٢٠) دقيقة على عملية الإزالة. تم جمع بيانات المختبر، وتم فحص الامتزاز حركيا. أظهرت النتائج أن امتزاز أيونات Pb على سطح $\alpha-Fe_2O_3$ المصنع تنطبق مع نموذج Langmuir، وبلغت معاملات (R^2) نسبة 98.65%. أظهرت أبحاث النماذج الحركية أن النموذج pseudo–2^{nd} order هو النموذج الأكثر ملائمة للعملية، حيث بلغ معامل (R^2) نسبة 99.97%. وكانت أعلى سعة امتزاز هي 165.2 ملجم رصاص/جرام مادة مازة.

الكلمات الدالة: الامتزاز الكيميائي، $\alpha-Fe2o3$ (الهيماتيت)، الترسيب المشترك، حمض البولي لاكتيك (PLA)، أيزو ثيرم الامتزاز، إزالة أيونات الرصاص (II)، معالجة مياه الصرف الصحي.